

ABSTRACT

STUDIES OF VECTOR BOSON SCATTERING IN THE SEMILEPTONIC ZV CHANNEL WITH THE CMS DETECTOR AT $\sqrt{s} = 13$ TEV

Ramanpreet Singh, Ph.D.

Department of Physics
Northern Illinois University, 2021
Vishnu Zutshi, Director

About Vector boson scattering (VBS)

NORTHERN ILLINOIS UNIVERSITY
DE KALB, ILLINOIS

SEPTEMBER 2021

**STUDIES OF VECTOR BOSON SCATTERING IN THE SEMILEPTONIC
ZV CHANNEL WITH THE CMS DETECTOR AT $\sqrt{s} = 13$ TEV**

BY

RAMANPREET SINGH
© 2021 Ramanpreet Singh

A DISSERTATION SUBMITTED TO THE GRADUATE SCHOOL
IN PARTIAL FULFILLMENT OF THE REQUIREMENTS
FOR THE DEGREE
DOCTOR OF PHILOSOPHY

DEPARTMENT OF PHYSICS

Dissertation Director:
Vishnu Zutshi

ACKNOWLEDGEMENTS

Acknowledge people here.

DEDICATION

To my family.

TABLE OF CONTENTS

	Page
LIST OF TABLES	vii
LIST OF FIGURES	viii
LIST OF APPENDICES	ix
Chapter	
1 INTRODUCTION	1
2 THE STANDARD MODEL	2
2.1 Standard model	2
2.1.1 Fundamental Particles	2
2.1.1.1 Fermions	2
3 THE LHC AND CMS EXPERIMENT	3
3.1 The Large Hadron Collider	3
3.1.1 Integrated Luminosity	5
3.2 The CMS Detector	6
3.2.1 The CMS Coordinate System	8
3.2.2 The Superconducting Magnet	9
3.2.3 The Tracking System	10
3.2.4 The Electromagnetic Calorimeter	11
3.2.5 The Hadronic Calorimeter	13
3.2.6 Muon Detector	14
3.2.7 Level 1 Trigger	16

Chapter	Page
3.3 High Granularity Calorimeter Upgrade	17
3.3.1 Technical Design	17
3.3.2 Scintillator Tiles	18
3.3.3 End of Life Scenario	18
4 EVENT SIMULATION AND RECONSTRUCTION	20
4.1 Track Reconstruction	20
4.2 Calorimeter Clustering	21
4.3 Particles Flow Candidates	21
4.3.1 Muons	21
4.3.2 Electrons and Photons	21
4.3.3 Hadrons and Jets	21
4.3.4 Missing transverse momentum	21
4.4 Monte Carlo Simulation	21
4.4.1 Generators	21
4.4.2 Hadronization	21
5 VBS MEASUREMENT IN $ZVJJ$ FINAL STATE	22
5.1 Dataset and Simulation	23
5.1.1 Data	23
5.1.2 MC Simulations	23
5.2 Event Selection	23
5.2.1 HLT Trigger	23
5.2.2 Lepton Selection	23
5.2.2.1 Muon	23
5.2.2.2 Electron	23

Chapter	Page
5.2.3 VBS Tagged Jets	23
5.2.4 V Jet Candidate	23
6 RESULTS	24
REFERENCES	25
APPENDICES	28

LIST OF TABLES

Table	Page
3.1 Standard physics luminosity for run-2	5
3.2 HGCAL scenarios comparison	19

LIST OF FIGURES

Figure		Page
3.1	A schematic of the CERN accelerator complex.	4
3.2	Cumulative delivered and recorded luminosity versus time for 2015–2018 proton-proton collisions	5
3.3	The CMS detector cutaway view	6
3.4	The CMS detector slice view	7
3.5	The picture of the CMS detector central part when lowered in underground cavern with superconducting magnet and iron yoke visible	9
3.6	The CMS pixel upgrade	11
3.7	The CMS ECAL schematic layout	12
3.8	The ECAL endcap quadrant assembled view	12
3.9	The first half of the barrel HCAL inserted into the superconducting solenoid (April 2006)	13
3.10	The HCAL depth segmentation after phase 1 upgrade	14
3.11	The quadrant view of CMS subdetectors layout, and the coverage of the muon detector DTs, CSCs, and RPCs highlighted	15
3.12	Overview of CE	17
3.13	HGCAL scenarios	18

LIST OF APPENDICES

Appendix	Page
A MACHINE LEARNING	28
B DATA ANALYSIS	30

CHAPTER 1

INTRODUCTION

CHAPTER 2

THE STANDARD MODEL

Introduction to Standard Model (SM), Effective Field Theory (EFT), Vector boson scattering (VBS), etc.

2.1 Standard model

Introduction to SM [1] goes here.

2.1.1 Fundamental Particles

About fundamental particles

2.1.1.1 Fermions

About fermions

CHAPTER 3

THE LHC AND CMS EXPERIMENT

The physics analysis is carried out using Compact Muon Solenoid (CMS) experiment at European Council for Nuclear Research (CERN) Large Hadron Collider (LHC) accelerator. This chapter provides overview of LHC and detail of CMS experiment and its sub-detectors for particle tracking and calorimetry.

3.1 The Large Hadron Collider

The LHC is the largest accelerator located at CERN in Geneva, Switzerland. The main LHC ring is 27 km in circumference and around 50 to 175 m underground. The LHC is built to collide protons at 14 TeV center-of-mass energy, LHC delivered proton-proton collisions at 7 and 8 TeV during run-1 (2010–2012), and at 13 TeV center-of-mass energy during run-2 (2015–2018) [2].

The Figure 3.1 describes CERN accelerator complex. The protons are sourced by ionizing hydrogen atoms and then fed into linear accelerator (LINAC). The LINAC accelerates the protons to 50 MeV and sent to the booster. Then the booster increases energy of protons to 1.4 MeV and feeds it to the proton syncrotron (PS) which further increases energy to 25 MeV and starts bunching them together with bunches 25 ns apart. Then the proton bunches are passed through super proton synchrotron (SPS) which increases energy to 450 MeV and finally sent to main LHC clockwise and counterclockwise rings where they are accelerated to

final energy required which is 6.5 TeV for both bunches going clockwise and counterclockwise to obtain collisions at 13 TeV center-of-mass energy.

The proton-proton collisions occurs at four different location where two general purpose detectors CMS and A Toroidal LHC Apparatus (ATLAS), and two specific purpose detector A Large Ion Collider Experiment (ALICE) and LHC-beauty (LHCb) are located.

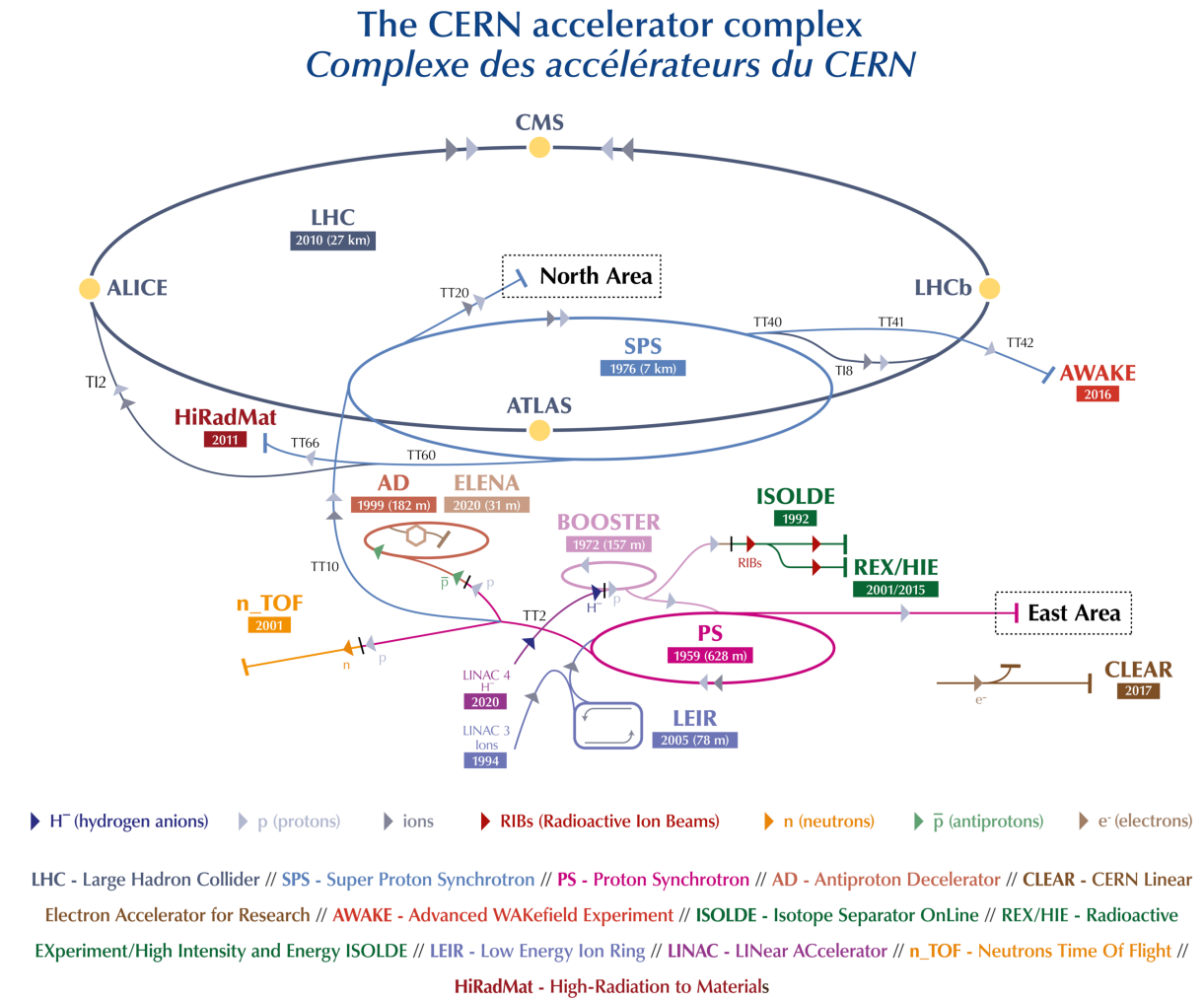


Figure 3.1: A schematic of the CERN accelerator complex [3]

3.1.1 Integrated Luminosity

The number of events generated in a collisions for a given process is

$$N = L\sigma \quad (3.1)$$

where σ is cross-section of the process and L is the luminosity of the LHC.

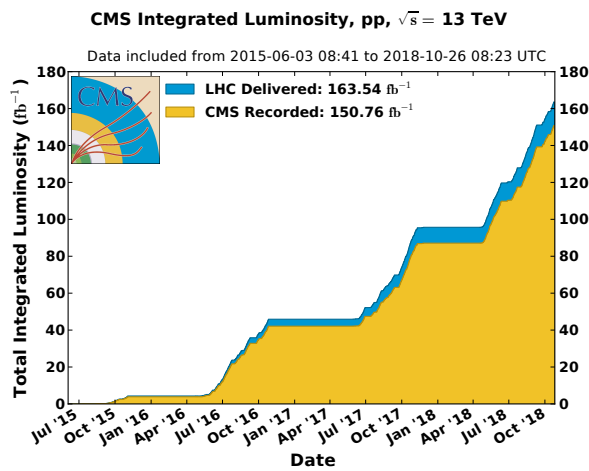


Figure 3.2: Cumulative delivered and recorded luminosity versus time for 2015–2018 proton-proton collisions [4]

Cumulative luminosity delivered and recorded by CMS during run-2 operation is shown in Figure 3.2. For run-2 standard physics analysis luminosity recorded during 2016–2018 is considered, and only runs certified as “golden” by CMS Luminosity physics object group (POG) for analysis are used. The total luminosity for run-2 standard physics is 137.19 fb^{-1} and separately for years in Table 3.1 [5–7].

Table 3.1: Standard physics luminosity for run-2

2016	2017	2018	run-2
35.92 fb^{-1}	41.53 fb^{-1}	59.74 fb^{-1}	137.19 fb^{-1}

3.2 The CMS Detector

The CMS detector is a general purpose detector. A cutaway view of the detector is shown in Figure 3.3. The detector is cylindrical with dimensions 21 meters long, and 15 meters in diameter, and the whole detector weighs about 14000 tonnes. The detector is built in slices with central region called “barrel”, and two closing end sides called “endcap”. A superconducting solenoid generates magnetic field of 3.8 T inside and 2 T outside, and to contain the magnetic field outside of solenoid and support structure of the detector massive steel yokes are used.

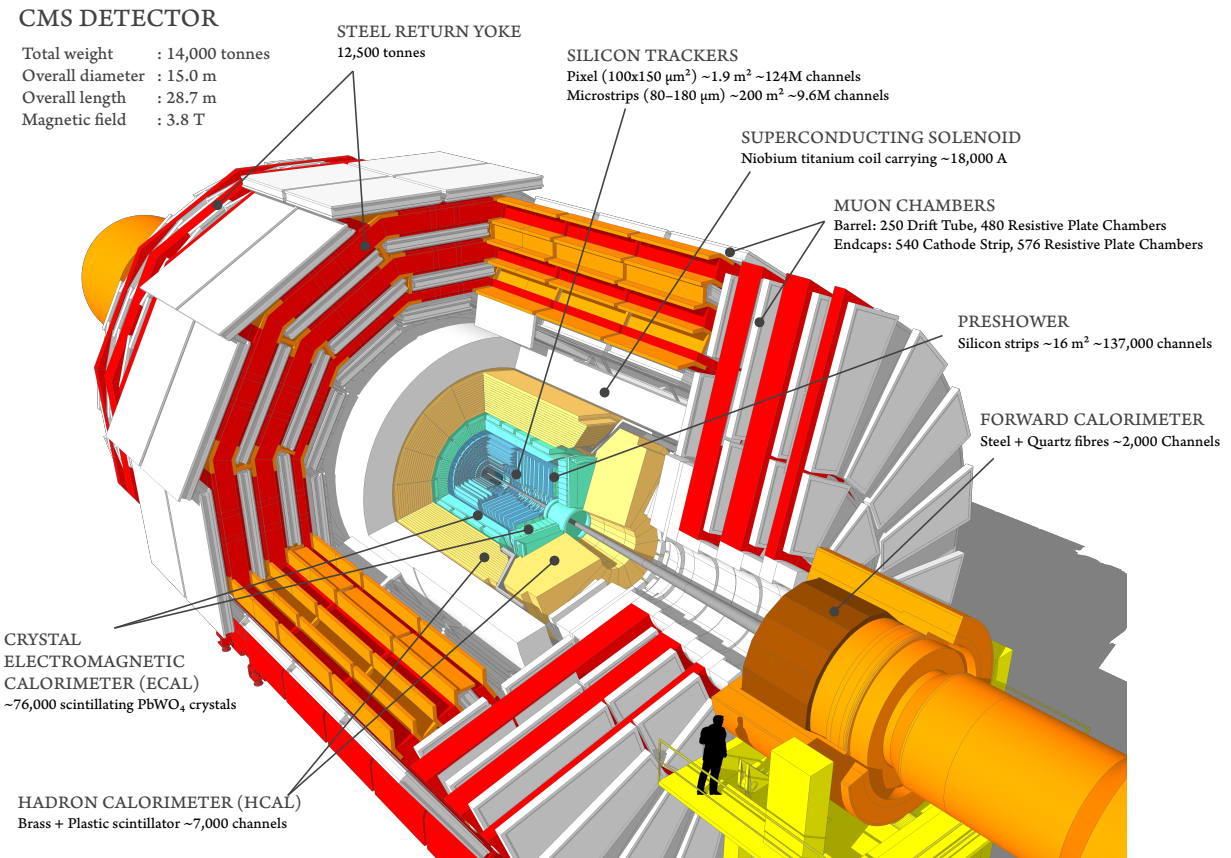


Figure 3.3: The CMS detector cutaway view [8]

The slice view of CMS in Figure 3.4 shows how different particles leave signature in CMS detector. Neutral particles such photons, neutrinos, and hadrons will leave no track in Silicon Tracker (ST), and are identified by only energy deposited or missing energy. Electrons are identified from the track in ST and energy deposit in Electromagnetic Calorimeter (ECAL), hadrons are heavier and they pass through ECAL and deposit their energy completely in Hadronic Calorimeter (HCAL), leaving only small fraction of energy in ECAL. Since muons are minimum ionizing particle (MIP), they pass through whole detector with very small fraction of energy deposit in ECAL and HCAL.

This section describes the subsystems of CMS detector. For detailed technical description refer to [9].

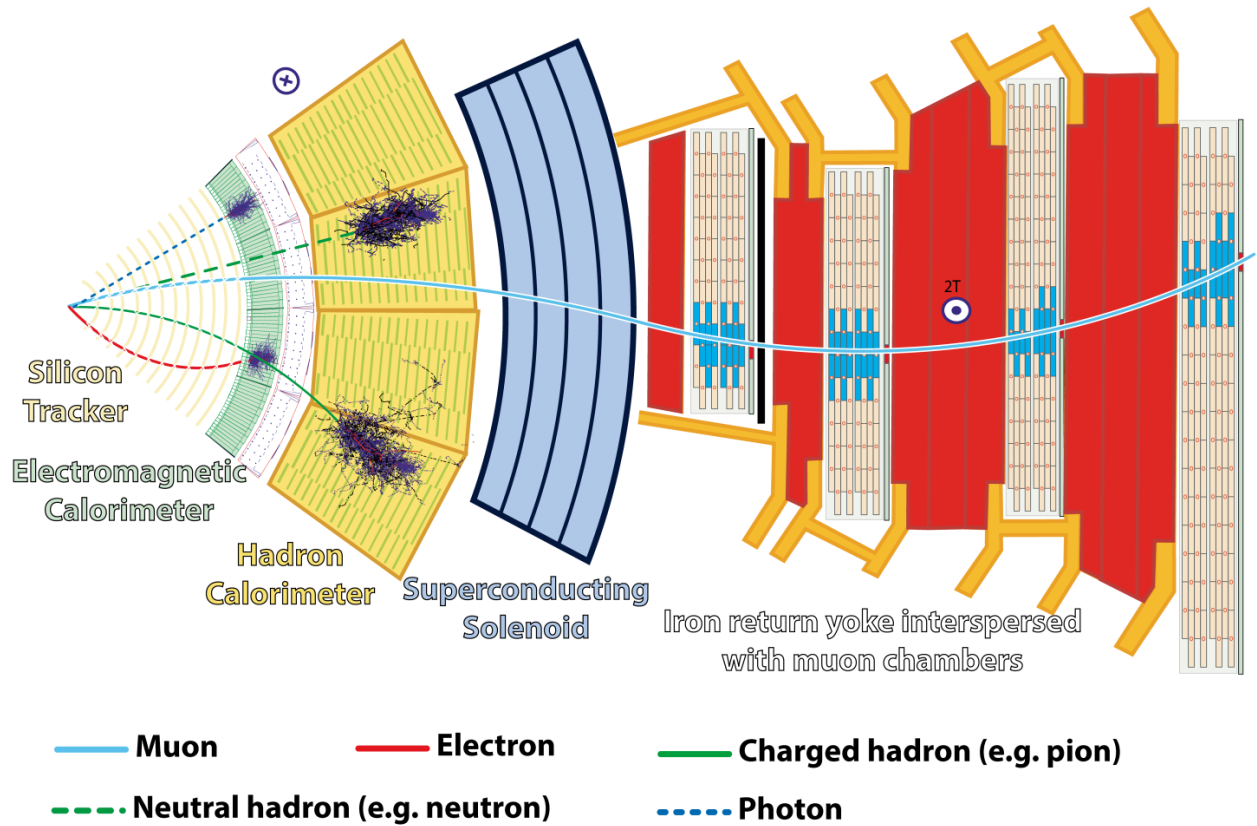


Figure 3.4: The CMS detector slice view [10]

3.2.1 The CMS Coordinate System

CMS uses interaction point (IP) of collisions as origin to define right-handed coordinate system. The z -axis is along the beamline, the x -axis points toward the center of the LHC, and the y -axis points upwards, toward Earth's surface. The transverse plane $x - y$ is used as to calculate most commonly used quantities like transverse momentum p_T and energy E_T .

To describe the direction of particles leaving the IP, azimuthal ϕ and polar θ angles are used. ϕ is measured around the beam axis, and θ is measured from the beam axis. In collider physics, pseudorapidity η (Lorentz invariant) is used to describe direction from beam pipe instead of θ as,

$$\eta = -\ln[\tan \theta/2] \quad (3.2)$$

and sometimes in terms of rapidity y as,

$$y = \frac{1}{2} \ln \frac{E + p_z}{E - p_z} \quad (3.3)$$

Particles kinematics can be completely described in terms of p_T , η , ϕ , and E_T or mass. The distance between the two particles ΔR in $\eta - \phi$ plane is described as,

$$\Delta R = \sqrt{(\Delta\eta)^2 + (\Delta\phi)^2} \quad (3.4)$$

3.2.2 The Superconducting Magnet

The superconducting magnet is the main part of the CMS detector, it is 12.5 meters long and 6.3 meters in diameter. The magnet is cooled to 4.5 K and 20 kA current flows through it to generate 3.8 T of magnetic field with stored energy of 2.6 GJ.

The Figure 3.5 shows visible superconducting magnet and iron yoke when part of CMS detector was lowered in the underground cavern during installation in 2007.

The key purpose of magnet is to determine the momentum and the sign of charged particles by bending them. The momentum resolution of the particles will decrease with increase in p_T , with constant 3.8 T magnetic field inside and it has momentum resolution of $\Delta p/p \approx 10\%$, which is enough to determine unambiguously the sign of muons with momentum of $\approx 1 \text{ TeV}/c$.

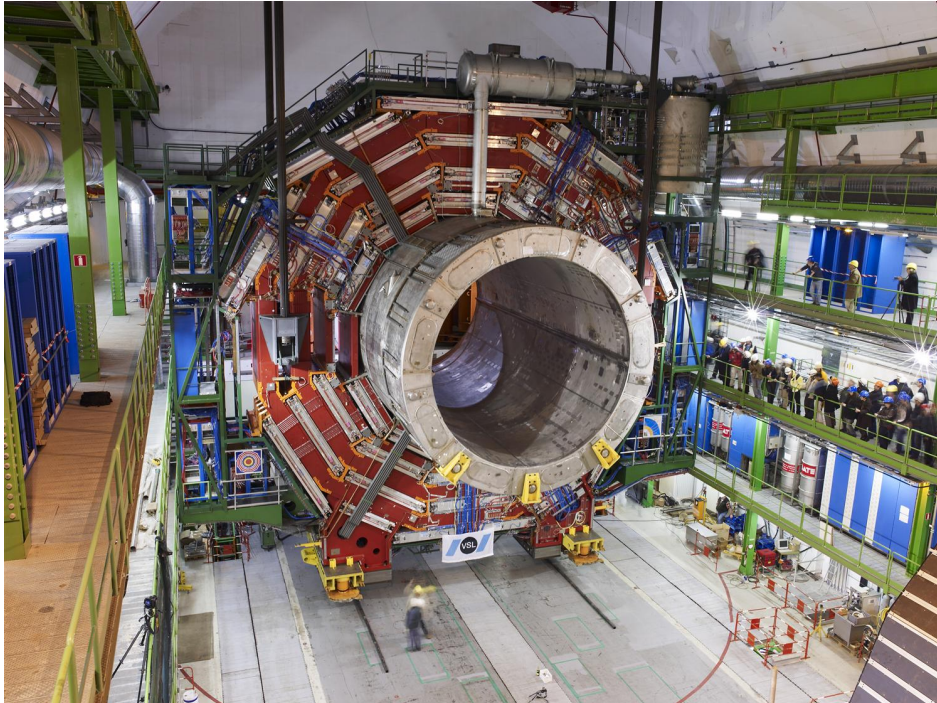


Figure 3.5: The picture of the CMS detector central part when lowered in underground cavern with superconducting magnet and iron yoke visible [11].

3.2.3 The Tracking System

The CMS tracking system ST is the innermost part of the detector, it is made up of pixel and strip detectors. The main goal of ST is to reconstruct the tracks of the charged particles with high precision in high pileup environment.

Silicon is most commonly used material for making tracking systems because of it's semiconductor properties, and high radiation hardness which is essential for the innermost detector. When a p-n junction is built on silicon substrate it creates a depletion zone with no charge carriers at the junction, and whenever a charged particle pass through the depletion zone it creates a electron-hole pair, and under reverse bias this electron-hole generates electrical signal. The CMS tracking consists of about 124 million channels of such junctions in pixel detector and 10 million in strip detector.

The pixel detector was upgraded in 2017 and the comparison of layers before and after the upgrade is shown in Figure 3.6. It is made up of four barrel layers and three endcaps, with nearest barrel layer being 3 cm away from beamline for precise measurement of IP. Because of the large number of pixel channels, the readout is done by Application-specific integrated circuits (ASICs).

The outermost part of ST detector is made of silicon strips. It allows large coverage by reducing number of readout channels. It has 10 layers in barrel region and 12 discs in endcap region. For better signal-to-noise ratio and radiation tolerance both pixel and strip operates at -20 °C.

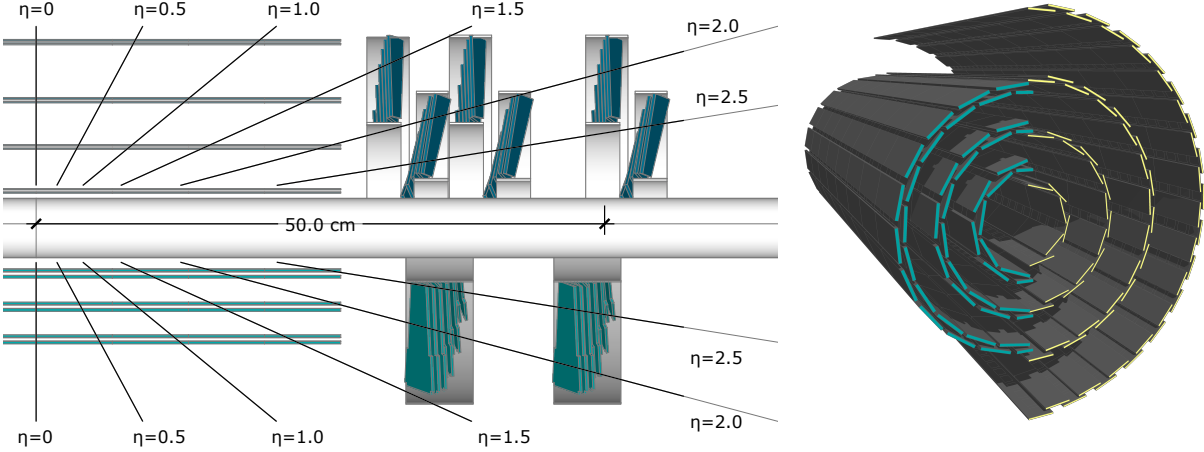


Figure 3.6: The CMS pixel upgrade. The left is cross sectional view of pixel detector layers before upgrade (bottom) and after Phase 1 upgrade (top). The right is view pixel barrel before upgrade (left) and after upgrade (right) [12].

3.2.4 The Electromagnetic Calorimeter

The ECAL active material is made of lead tungstate (PbWO_4) scintillating crystals and two layers silicon strip for preshower in front of the endcaps. The crystals in central barrel section are mounted in quasi-projective geometry pointing towards IP and covers $|\eta| < 1.48$, and two endcaps extends the coverage to $|\eta| = 3.0$. The schematic layout of ECAL is shown in Figure 3.7 and the picture of endcap quadrant when assembled in Figure 3.8

The main purpose of ECAL is to determine energy and positions of electromagnetically interacting particles. To determine particle need to completely deposit their energy, except electron and photons all other particles pass through ECAL crystals with only small fraction of energy signature in crystals. When electron and photon interacts with PbWO_4 it starts the process of electromagnetic shower and continues until the energy the energy of the incident particle is below threshold, which is about 1 MeV.

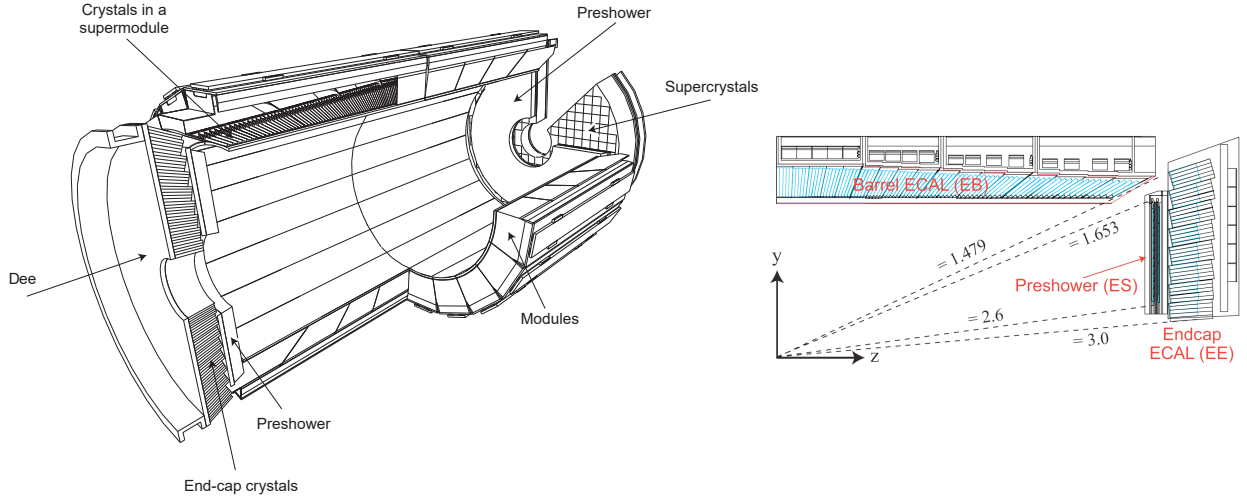


Figure 3.7: The CMS ECAL schematic layout. The left is schematic showing arrangement of superclusters in barrel and endcap (with preshower layers). The right is $y - z$ plane quarter view of ECAL layout [13].

The resolution of the ECAL energy measurements can be described as,

$$\left(\frac{\sigma}{E}\right)^2 = \left(\frac{S}{\sqrt{E}}\right)^2 + \left(\frac{N}{E}\right)^2 + C^2 \quad (3.5)$$

where S is the stochastic term, N is related to the noise, and C is a constant offset.

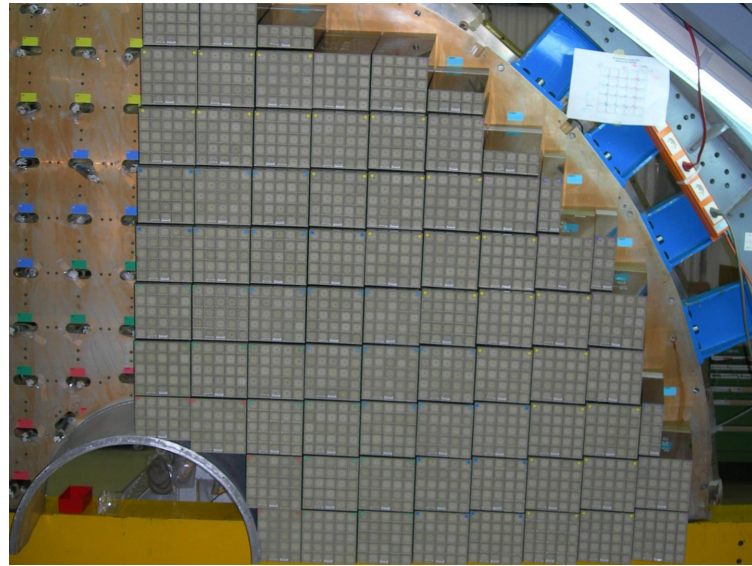


Figure 3.8: The ECAL endcap quadrant assembled view [14].

3.2.5 The Hadronic Calorimeter

HCAL is last subdetector inside solenoid after ECAL and the first half of barrel HCAL inserted is shown in Figure 3.9. Similar to ECAL the purpose of HCAL is to shower hadrons, and measure their energy and position. HCAL is made up of towers pointing towards IP and each tower is made up of sampling layers with alternating layers of plastic scintillator and brass. Brass acts as absorber in HCAL and causes hadrons to shower, then from the light output of scintillator receiving secondary shower particles gives the amount of energy deposit in each layer. In phase 1 upgrade the HCAL was upgraded to give energy deposit as function of depths and the depth segmentation schematic is show in Figure 3.10 and the details of upgrade are in technical design report [15].



Figure 3.9: The first half of the barrel HCAL inserted into the superconducting solenoid (April 2006) [16].

HCAL consists barrel (HB) and two endcaps (HE) located inside solenoid. These two subsystems combined cover region $|\eta| = 3.0$, which is most of physics analysis done in CMS. There are two other subsystems of HCAL outside solenoid, a forward HCAL (HF) and outer barrel HCAL (HO). HO was added to ensure there is no leak from the particles that make past the solenoid. HF extends the coverage to $|\eta| = 5.0$ and is based Cherenkov radiation principle unlike other subsystems of HCAL, and it uses quartz fiber as active material with steel absorbers. HF is used most commonly used by heavy ion analysis.

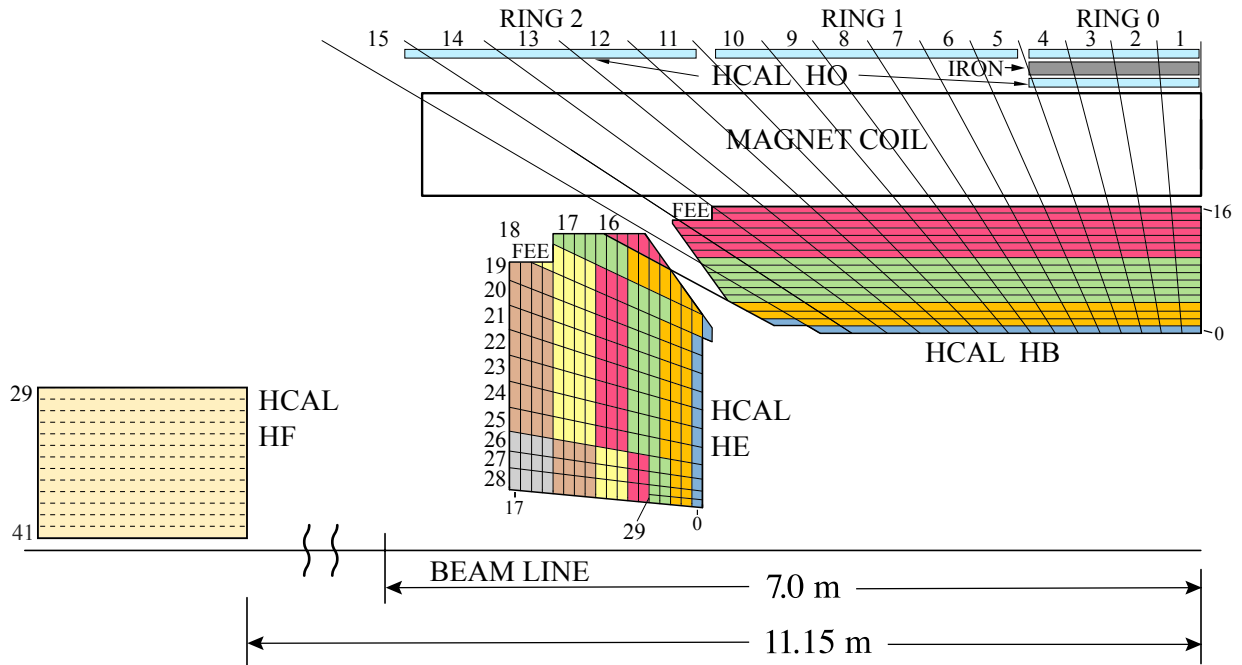


Figure 3.10: The HCAL depth segmentation after phase 1 upgrade [17].

3.2.6 Muon Detector

The outermost subsystem in the CMS detector is the muon detector. Unlike electrons, muons are MIPs, they do not lose much of their energy while passing through tracker, calorimeter and solenoid. Muon detector is build to identify, measure momentum and trigger

the events with muons. Like other subsystems, muon detector consists of barrel and endcap detector and schematic layout is highlighted in Figure 3.11.

The muon detector consists of three subsystems drift tubes (DTs), cathode strip chambers (CSCs) and resistive plate chambers (RPCs).

The DTs are wire gas detectors filled with Argon and composed of many tube cells of about 4 cm. Muon passing through these tubes ionizes Argon and free electron is detected with wires as cathode. Each DT is about 2 meters by 2.5 meters in size, and there are four layers of the DTs interleaved with iron yoke parallel to the beam pipe in barrel region. The drift time is the order of about 380 ns.

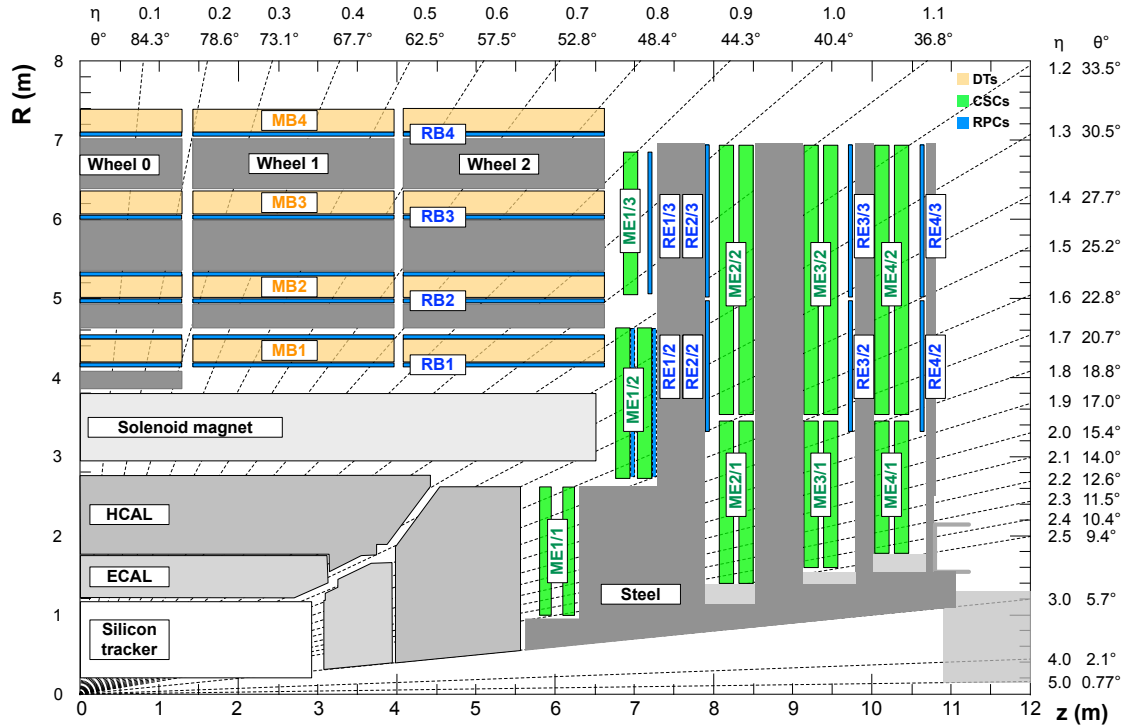


Figure 3.11: The quadrant view of CMS subdetectors layout, and the coverage of the muon detector DTs, CSCs, and RPCs highlighted [18].

The CSCs are based on same principle as DTs, and are made of multi-wire proportional chambers consisting of 6 anode planes interleaved with 7 cathode planes. They have time

resolution smaller than 5 ns. The CSCs are used in endcap region, where radiation hardness is required, and non uniform magnetic field does neutrinos effects the the measurement.

The RPCs are made up of two high resistive parallel plates, with oppositely charged plates and gas volume between them. When a charged particles passes through it and ionizes the gas, it creates an avalanche and charge is collected by metallic readout strips. RPCs have poor position resolution but fast readout of the order of 1 ns, which is fast compared to DTs, this is the reason there are 1 or 2 RPCs attached to both DTs, and CSCs.

3.2.7 Level 1 Trigger

Since proton-proton collisions happens every bunch crossing which is 25 ns apart, which is equivalent to 40 MHz collisions rate. At this collisions rate, the data storage required will be enormous and CMS can only record up to 1000 events per second. Since most of events does not contain interesting physics events, they can be thrown away. To do this CMS has two tier trigger system Level-1 Trigger (L1T), and High Level Trigger (HLT).

The L1T is the foremost electronic processing system through which event information is processed before it is passed to second trigger system HLT. The L1T is designed to make fast decisions in about $3.8\ \mu s$, and only uses ECAL, HCAL and muon system to make decision. L1T cut downs the data rate from 40 MHz to 100 kHz. The L1T electronics is placed next to the detector in underground cavern for fast transfer of data.

The HLT further reduces the data rate from 100 kHz to about 1 kHz using a computer farm with nearly 26000 cores. HLT uses all the available information from the event to make decision in about 300ms. HLT is modular by design to allow the use of information from different systems to construct multiple paths called HLT paths, for example the single muon

HLT path will save event with at least one muon passing the selection criteria set in HLT path. Events passing at least on HLT path are save for offline physics analysis.

3.3 High Granularity Calorimeter Upgrade

About High Granularity Calorimeter (HGCAL) Upgrade

3.3.1 Technical Design

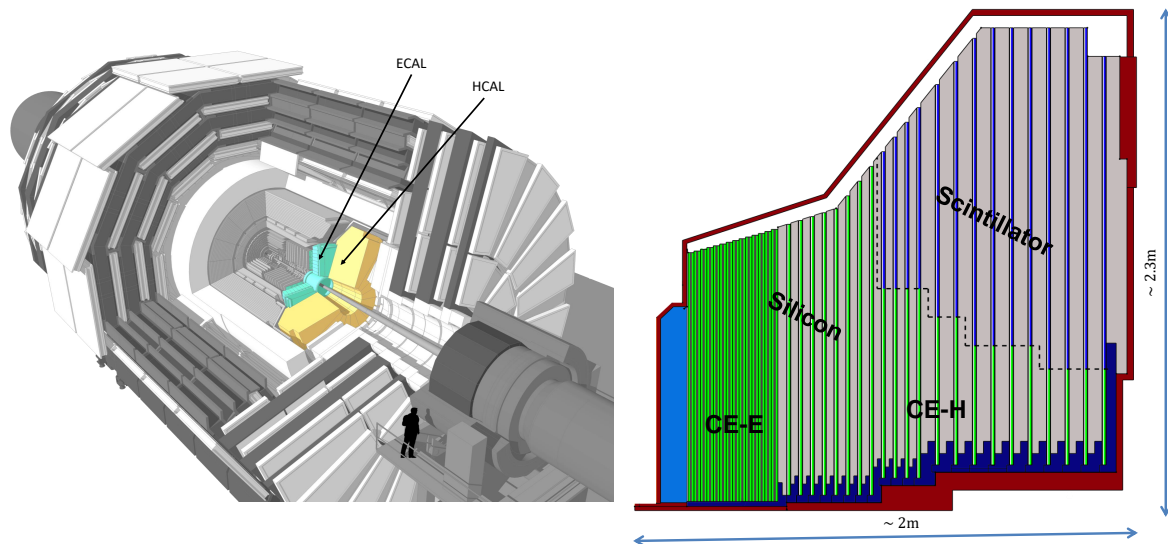


Figure 3.12: Overview of CE [19, 20]

3.3.2 Scintillator Tiles

3.3.3 End of Life Scenario

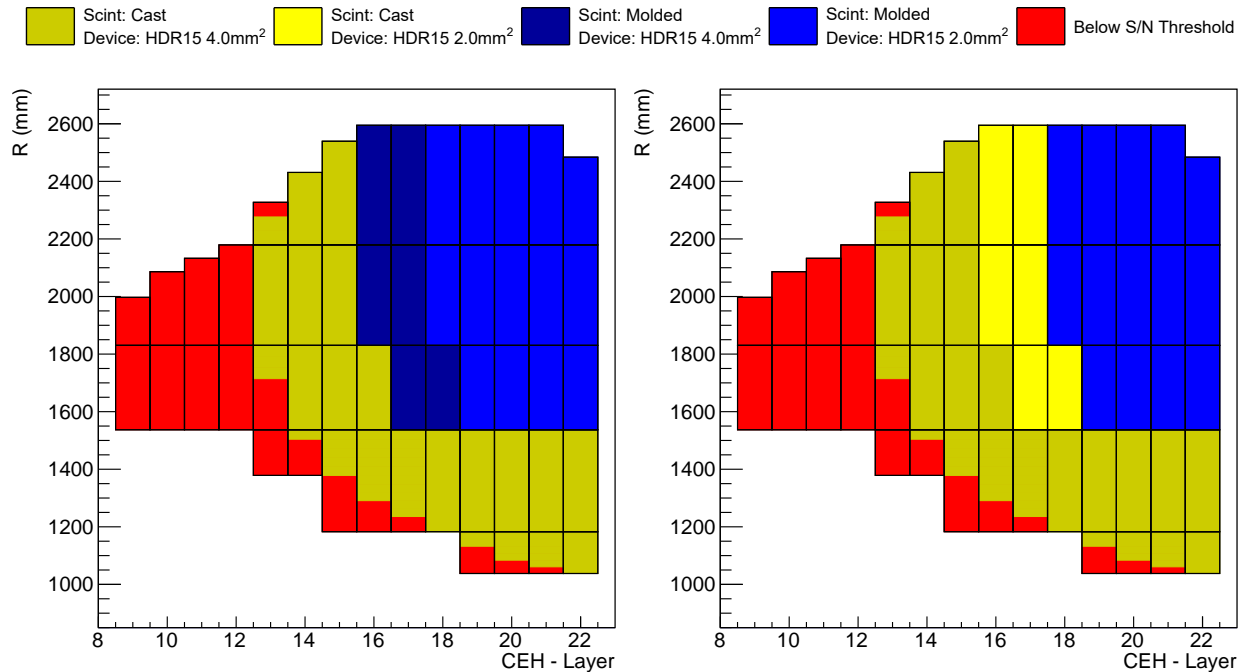


Figure 3.13: HGCAL scenarios

Table 3.2: HGCAL scenarios comparison

		Scene A	Scene B
Cast Scintillator	Cell Count	148, 608	176, 256
	Total Area	185.13 m ²	239.45 m ²
	Percentage	50.6 %	65.5 %
Injection Molded Scintillator	Cell Count	91, 008	63, 360
	Total Area	180.5 m ²	126.18 m ²
	Percentage	49.4 %	34.5 %
SiPMs Count	2 mm ²	63, 360	91, 008
	4 mm ²	100, 224	148, 608

CHAPTER 4

EVENT SIMULATION AND RECONSTRUCTION

The proton-proton collision at LHC produces shower of particles, before the event information can be easily used in an analysis, the data collected goes through iterative process of reconstruct particles produced in collision. CMS uses particle flow (PF) algorithm to reconstruct 4-vectors of muons, electrons, photons, hadrons, jets and missing transverse momentum [21].

To analyze the data collected and compare it with theoretical model, events are simulated using Monte Carlo (MC) event generators and are passed through detector simulation and PF so that MC events can be treated same as real events.

This chapter describes the basic ingredients for object reconstruction, PF candidates and MC event generators used in this analysis.

4.1 Track Reconstruction

Kalman Filtering (KF) [22] GEANT4

4.2 Calorimeter Clustering

4.3 Particles Flow Candidates

4.3.1 Muons

4.3.2 Electrons and Photons

4.3.3 Hadrons and Jets

4.3.4 Missing transverse momentum

4.4 Monte Carlo Simulation

4.4.1 Generators

4.4.2 Hadronization

CHAPTER 5

VBS MEASUREMENT IN $ZVJJ$ FINAL STATE

Analysis of VBS

5.1 Dataset and Simulation

5.1.1 Data

5.1.2 MC Simulations

5.2 Event Selection

5.2.1 HLT Trigger

5.2.2 Lepton Selection

5.2.2.1 Muon

5.2.2.2 Electron

5.2.3 VBS Tagged Jets

5.2.4 V Jet Candidate

CHAPTER 6

RESULTS

REFERENCES

- [1] C. N. Yang and R. L. Mills. “Conservation of Isotopic Spin and Isotopic Gauge Invariance”. *Phys. Rev.* 96 (1 Oct. 1954), pp. 191–195. doi: 10.1103/PhysRev.96.191. URL: <https://link.aps.org/doi/10.1103/PhysRev.96.191>.
- [2] L. Evans and P. Bryant. “LHC Machine”. *Journal of Instrumentation* 3.08 (Aug. 2008), S08001–S08001. doi: 10.1088/1748-0221/3/08/s08001.
- [3] E. Mobs. “The CERN accelerator complex - 2019” (July 2019). Accessed August 16, 2021. URL: <http://cds.cern.ch/record/2684277/files/>.
- [4] Public CMS Luminosity Information. “Cumulative delivered and recorded luminosity versus time for run-2 pp data” (2018). Accessed August 17, 2021. URL: <https://twiki.cern.ch/twiki/bin/view/CMSPublic/LumiPublicResults>.
- [5] The CMS Collaboration. “CMS Luminosity Measurements for the 2016 Data Taking Period” (2017). URL: <https://cds.cern.ch/record/2257069>.
- [6] The CMS Collaboration. “CMS luminosity measurement for the 2017 data-taking period at $\sqrt{s} = 13$ TeV” (2018). URL: <https://cds.cern.ch/record/2621960>.
- [7] The CMS Collaboration. “CMS luminosity measurement for the 2018 data-taking period at $\sqrt{s} = 13$ TeV” (2019). URL: <https://cds.cern.ch/record/2676164>.
- [8] T. Sakuma. “Cutaway diagrams of CMS detector” (May 2019). Accessed August 17, 2021. URL: <https://cds.cern.ch/record/2665537>.
- [9] The CMS Collaboration. “The CMS experiment at the CERN LHC”. *Journal of Instrumentation* 3.08 (Aug. 2008), S08004–S08004. doi: 10.1088/1748-0221/3/08/s08004. URL: <https://doi.org/10.1088/1748-0221/3/08/s08004>.

- [10] The CMS Collaboration. “CMS Detector Slice” (Jan. 2016). Accessed August 18, 2021. URL: <https://cds.cern.ch/record/2120661>.
- [11] M. Brice and C. Marcelloni. “The central part of CMS is lowered” (Feb. 2007). Accessed August 22, 2021. URL: <https://cds.cern.ch/record/1020311>.
- [12] T. Sakuma. “SketchUp Drawings of the Phase 1 pixel detector alongside the current pixel detector” (June 2012). Accessed August 17, 2021. URL: <https://cms-docdb.cern.ch/cgi-bin/PublicDocDB>ShowDocument?docid=6473>.
- [13] The CMS Collaboration. “The CMS ECAL performance with examples”. *Journal of Instrumentation* 9.02 (Feb. 2014), pp. C02008–C02008. DOI: [10.1088/1748-0221/9/02/c02008](https://doi.org/10.1088/1748-0221/9/02/c02008).
- [14] The CMS Collaboration. “Images of CMS ECAL Endcap (EE)” (Nov. 2008). Accessed August 22, 2021. URL: <https://cds.cern.ch/record/1431479>.
- [15] J. Mans et al. “CMS Technical Design Report for the Phase 1 Upgrade of the Hadron Calorimeter” (Sept. 2012). URL: <https://cds.cern.ch/record/1481837>.
- [16] The CMS Collaboration. “Images of the CMS HCAL Barrel (HB)” (2008). Accessed August 22, 2021. URL: <https://cds.cern.ch/record/1431485>.
- [17] The CMS Collaboration. “HCAL Depth Segmentation Phase 1 Upgrade” (2012). Accessed August 22, 2021. URL: <https://home.fnal.gov/~chlebana/CMS/Phase1>.
- [18] The CMS Collaboration. “Performance of the CMS Muon Detectors in early 2016 collision runs” (2016). Accessed August 22, 2021. URL: <https://twiki.cern.ch/twiki/pub/CMSPublic/MuonDPGPublic160729>.
- [19] D. Barney. “Overview slide of CE with main parameters” (Oct. 2019). Accessed August 24, 2021. URL: <https://cms-docdb.cern.ch/cgi-bin/PublicDocDB>ShowDocument?docid=13251>.

- [20] D. Barney and T. Sakuma. “Sketchup images highlighting the sub-detectors” (Sept. 2017). Accessed August 24, 2021. URL: <https://cds.cern.ch/record/2628519>.
- [21] The CMS Collaboration. “Particle-flow reconstruction and global event description with the CMS detector”. *Journal of Instrumentation* 12.10 (Oct. 2017), P10003–P10003. DOI: [10.1088/1748-0221/12/10/p10003](https://doi.org/10.1088/1748-0221/12/10/p10003).
- [22] W. Adam et al. *Track Reconstruction in the CMS tracker*. Tech. rep. Geneva: CERN, Dec. 2006. URL: <https://cds.cern.ch/record/934067>.

APPENDIX A

MACHINE LEARNING

Write about Machine learning (ML), Multivariate analysis (MVA), Boosted decision tree (BDT), etc.

APPENDIX B

DATA ANALYSIS

Data Analysis Code and Stuff